Eigen Energies and the Statistical Distributions of the Rovibrational Levels of the Bosonic van der Waals Argon Trimer†

Anton Gagin,† Evgeny Yarevsky,† Moses Salci,‡ and Nils Elander*,‡

Department of Computational Physics, St. Petersburg State University, 198504 St. Petersburg, Russia, and AlbaNova University Center, Department of Physics, Stockholm University, SE-106 91 Stockholm, Sweden

Received: May 31, 2009; Revised Manuscript Received: October 5, 2009

The eigen energies and the statistical distributions of the rovibrational levels ($J = 0-2$) of the bosonic van der Waals argon trimer were calculated using a full angular momentum three-dimensional finite element method. The influence of interatomic potentials on the vibrational levels and statistical properties of the trimer was discussed.

Introduction

van der Waals (vdW) clusters are in general characterized as weakly bound complexes of closed shell atoms or molecules with relatively small dissociation energies of typically a few cm^{-1} to about 1000 cm^{-1}, and with large bond lengths about 3−4 Å.[1,2] Due to these factors, vdW clusters are only stable at very low temperatures. Many of them may dissociate by a single infrared photon by the breaking of a vdW bond. The interaction potentials of these complexes along the vdW bonds are dominated by long-range attractive dispersion forces of dipole−dipole nature, the interaction potential behaving as r^{-6}, where r is the vdW bond distance. Due to the relatively weak coupling between the vdW modes, a weak restoring force is present along the vdW bond distance, making the complex diffuse and unstructured in space.

The importance of the study of small weakly bound vdW clusters cannot be overemphasized. Important information such as many-body interaction potentials may be revealed, which in turn may be of fundamental importance in the study of larger clusters of atoms, such as superfluidity of finite-sized systems.[3] Besides this, the study of small vdW clusters may give ready information on fundamental quantum mechanical effects occurring in few-body physics.

Accurate calculations of small vdW clusters are, however, a challenging problem mainly due to their strongly anharmonic potential surfaces implying diffuse and delocalized probability distributions of the wave function in the configuration space. As such, calculations of atomic vdW trimers provide a challenge for any formal/numerical method.[4−12]

Recently the argon trimer Ar_3 was addressed in studies for a search of the optimal sum of two-body pair potentials model using variational expansion over distributed Gaussian functions.[9] This paper also discusses the influence of three-body so called Axilrod−Teller corrections to the potential.[13,14] Both Axilrod−Teller corrections and ab initio three-body forces are further discussed in ref 15. This paper also describes higher ($J \neq 0$) angular momentum states in a hyperspherical full angular momentum formalism with the discrete variable representation (DVR) including Coriolis forces. The maximum angular momentum studied is $J = 6$. In refs 16 and 17 the distributed Gaussian functions method is used to describe symmetry assignments of rotational energy levels assuming the vibration−rotation separation. States with the maximum angular momentum quantum number up to $J = 20$ are studied in ref 17.

In this report, we study the bosonic vdW argon trimer Ar_3 using an exact Hamiltonian in the full angular momentum representation numerically realized with a finite element method.[7] The bound state results for $J = 0$ with both Morse-type and semiempirical potentials are compared to previous studies.[8−12,15] Structural properties are calculated and compared to known results. Hence we have also calculated the rovibrational states up to $J = 2$ for both positive and negative parities.

Compared to lighter trimers, the argon trimer has relatively many vibrational states, and even more rovibrational ones. Hence it is meaningful to discuss the statistical properties of the trimer energy levels. The studies of the Ar_3 statistical properties are available in the literature[12,18] for some potentials. However, in the same way as the choice of an interatomic potential affects positions of individual levels, it should also affect the statistical properties of the system. Hence, here we perform a comparative study of two potentials from this point of view.

We estimate the nearest neighbor level spacings distribution, the spectral rigidity, and some correlation coefficients for the spectrum and compare them for the Morse and semiempirical potentials.

Theoretical Approach

The wave function of a three-body quantum system with the total angular momentum J can be expanded in terms of symmetrical Wigner D-functions.[19] Jacobi coordinates are chosen for the body-fixed coordinate $\vec{R} = (x, y, z)$, where x is the distance between particles 2 and 3, y is the distance between particle 1 and the center of mass of the pair (2, 3), and ϕ is the angle between the vectors $\vec{x}$ and $\vec{y}$. The Schrödinger equation for the trimer, in the terms of the wave function components $\psi^{(Js)}$, can be written as[19,20]

† Part of the "Vincenzo Aquilanti Festschrift".

* E-mail: elander@physto.se.
† St. Petersburg State University.
‡ Stockholm University.

10.1021/jp905109c
Published on Web 11/02/2009

$$-i\sqrt{1+\delta_{s1}}\frac{3\lambda_{-}(J,s)}{4my^2}\left[\frac{\partial}{\partial\phi}+(1-s)\cot\phi\right]\psi^{(Js-1)}+$$
$$[-\Delta_x^{(s)}-\Delta_y^{(s)}+V(x,y,\phi)-E]\psi^{(Js)}-$$
$$i\sqrt{1+\delta_{s0}}\frac{3\lambda_{+}(J,s)}{4my^2}\left[\frac{\partial}{\partial\phi}+(1+s)\cot\phi\right]\psi^{(Js+1)}=0 \quad (1)$$

The helicity quantum number, s, varies as $s = 0, ..., J$ for positive parity, and as $s = 1, ..., J$ for negative parity. The diagonal components $\Delta_{x,y}^{(s)}$ of the kinetic energy operator are defined as follows

$$-\Delta_x^{(s)} = -\frac{1}{mx^2}\left[x\frac{\partial^2}{\partial x^2}x+\left(\frac{\partial^2}{\partial\phi^2}+\cot\phi\frac{\partial}{\partial\phi}-\frac{s^2}{\sin^2\phi}\right)\right]$$
$$-\Delta_y^{(s)} = -\frac{3}{4my^2}\left[y\frac{\partial^2}{\partial y^2}y-(J(J+1)-2s^2)+\left(\frac{\partial^2}{\partial\phi^2}+\cot\phi\frac{\partial}{\partial\phi}-\frac{s^2}{\sin^2\phi}\right)\right]$$

Here $\lambda_{\pm}(J, s) = [J(J+1) - s(s \pm 1)]^{1/2}$ and $\psi^{(J-1)} \equiv 0$, and m is the mass of the Ar atom.

Potential Energy Surface. The potential energy surface in eq 1 can be decomposed into the sum of pairwise-additive interactions

$$V(\vec{R}) = V_p(r_{12}) + V_p(r_{23}) + V_p(r_{31}) \quad (2)$$

where r_{12}, r_{23}, and r_{31} are the interatomic distances. These distances are expressed in the terms of Jacobi coordinates as

$$r_{23} = |\vec{r}_2 - \vec{r}_3| = x$$

$$r_{12} = |\vec{r}_1 - \vec{r}_2| = (y^2 + xy\cos\phi + x^2/4)^{1/2}$$

$$r_{31} = |\vec{r}_3 - \vec{r}_1| = (y^2 - xy\cos\phi + x^2/4)^{1/2}$$

In the present work we do not take into account a relatively small nonadditive contribution to the total interaction (2).[21] This short-range three-body term raises the ground state up to 3 cm^{-1}, but its influence decreases gradually with the increase of the vibrational excitation down below 1 cm^{-1} for the 20th symmetric states.[9,15]

To describe the Ar−Ar interaction, we have selected two potentials: the semiempirical HFDID1 potential of Aziz,[22] and the Morse potential.[10] The Aziz potential[22] results in a well depth of 103.3 cm^{-1} and an equilibrium distance $r_m = 3.757$ Å. The total potential 2 has a well depth 310 cm^{-1} and a barrier to linearity at the level −170 cm^{-1}. The two-body dissociation threshold for the $Ar_3 \rightarrow Ar_2 + Ar$ channel lies at −84.75 cm^{-1}.

The Morse potential is represented in the standard form

$$V_{Morse}(r) = D(e^{-2\alpha(r-r_e)} - 2e^{-\alpha(r-r_e)}) \quad (3)$$

with the following parameters:[10] $\alpha = 0.908\,596\,909$ $Å^{-1}$, $D =$ 99 cm^{-1}, and $r_e = 3.757$ Å. The well depth and the equilibrium distance of the Morse potential coincide with those of the Aziz potential. Due to different shapes of the potentials, however, the corresponding dissociation energies differ. It is equal to 83.93 cm^{-1} for the Morse potential and to 84.75 cm^{-1} for the Aziz potential compare to the experimental result 84.47 cm^{-1}.[23]

Numerical Approach. The calculations have been performed using the three-dimensional finite element method. The method coincides with that used in ref 20 for the neon trimer calculations. This implementation is discussed in refs 24 and 25. The three-dimensional configuration space is divided into a number of elements. In each element, the component $\psi^J(x,y,\phi)$ of the total wave function is expanded into a sum of local basis functions

$$\psi^J(x,y,\phi) = \sum_{i,m} c_{i,m} f_{i,m}(x,y,\phi) \quad (4)$$

Here index i numbers the element, and m indicates the local basis function in each element. Expansion 4 reduces the Schrödinger equation to the generalized eigenvalue problem

$$\tilde{H}c = E\tilde{S}c$$

where vector $\vec{c}$ determines expansion coefficients $c_{i,m}$. This problem was solved using the Arnoldi method[26] with the shift-invert approach. The PARDISO library[27] was used for the solution of the linear system of equations.

Calculations, Results, and Discussion

Calculations. The bosonic argon trimer belongs to D_{3h} symmetry group. However, the use of Jacobi coordinate system reduces Ar_3 molecular symmetry group to C_{2v}; i.e., only the permutation of particles 2 and 3 would not affect the Hamiltonian in the new coordinates. Thus the total wave function of the system can be chosen symmetric or antisymmetric with respect to the permutation of atoms 2 and 3. The Hamiltonian matrix splits into two blocks, one symmetric and one antisymmetric. The first block contains totally symmetric A_1 states and the first component of two-fold degenerate E states, while the second contains totally antisymmetric A_2 states with the second component of degenerate E states.[10,12] The computational advantage of the wave function symmetry is the possibility to divide calculation into two parts, using only odd or even Legendre polynomials among z-direction and thus computing antisymmetric or symmetric wave functions, respectively.

The mesh construction resembles that for our calculations of the neon trimer.[20] However, the argon trimer has considerably more energy levels, so the calculation accuracy has been essentially improved. In total, 38 elements were used to describe x and y coordinates within the interval [0, 18] au. The Legendre polynomials up to a degree of 7 weighted by an exponential function were used as local basis functions in the directions x and y. One element only was used to describe the ϕ-direction. Basis functions were chosen to be the Legendre polynomials up to a degree of 30. This mesh resulted in a sparse matrix with the size 98 553. Matrix elements of the potential were calculated using 15 Gauss-quadrature points in the x and y directions, and 45 points in the ϕ-direction.

Results for $J = 0$. In the present work we have calculated energy levels and average root mean square (rms) radii for both the Aziz and Morse potentials. To make the comparison with previous results easier, we have used the argon mass $m_{Ar} =$ 39.9624 amu for the Morse potential, and $m_{Ar} = 39.948$ amu for the Aziz potential.

TABLE 1: Vibrational Energy Levels (cm^{-1}) for Ar_2

v	Morse	Aziz
0	–83.93	–84.75
1	–57.52	–59.04
2	–36.09	–38.38
3	–19.63	–22.90
4	–8.14	–11.99
5	–1.63	–5.16
6		–1.59
7		–0.22

TABLE 2: Ar_3 Vibrational Energy Levels (cm^{-1}) for the Morse Potential

		this work				
	v	A_1/E	A_2/E	ref 9	ref 11	ref 10
A_1	0	–252.44		–252.45	–252.43	–252.45
E	1	–229.33	–229.33			
A_1	2	–220.94		–220.94	–220.92	–220.94
A_1	3	–208.24		–208.24	–208.22	–208.24
E	4	–208.04	–208.03			
E	5	–201.05	–201.06			
A_1	6	–193.73		–193.74	–193.72	–193.75
E	7	–190.74	–190.73			
A_1	8	–189.06		–189.06	–189.04	–189.07
A_2	9		–185.82			
E	10	–182.92	–182.90			
A_1	11	–181.36		–181.40	–181.38	–181.41
E	12	–179.06	–179.09			
A_1	13	–177.26		–177.27	–177.24	–177.28
E	14	–174.77	–174.79			
A_1	15	–171.70		–171.72	–171.67	–171.72
E	16	–171.58	–171.58			
A_1	17	–168.90		–168.90	–168.63	–168.90
E	18	–168.89	–168.89			
A_1	19	–167.99		–168.00	–167.72	–168.00

While these potentials have the same position and depth of the minimum, the number and the values of energy levels differ already for the argon dimer; see Table 1. The results for the Morse potential coincide with those calculated in ref 9.

For the argon trimer, we have obtained first 267 symmetric states (those include A_1 levels and the first component of E states) and 217 antisymmetric states (A_2 levels and the second component of E states) below the dissociation channel for the Morse potential. For the HFDID1 potential, we have obtained the first 325 symmetric and 271 antisymmetric states. It is worth noting that the energy calculations near the two-body threshold are less accurate due to a complicated structure and large size of the corresponding wave functions. As our calculations are variational, the exact numbers of energy levels may thus only be bigger than those mentioned above. Some examples of the computed energy levels are given in Tables 2 and 3. The differences between symmetric and antisymmetric parts of E states are within the 0.05 cm^{-1} limit for all calculations.

Coming to the convergence of our results, we should state that the quantitative estimate of the error is always a complicate task. Hence we try to estimate the errors with different arguments. The first estimate gives the difference between the energies of symmetric and antisymmetric parts of E states. Clearly, the total error cannot be lesser than this difference, which results in the 0.05 cm^{-1} error. Other estimation is based on the extrapolation of the energy levels when the number of the expansion function is increased.[28] Comparing the calculated energy levels with the extrapolated ones, we can use their difference as a measure of the error. This approach gives us the error 0.01 cm^{-1} for first 20 levels. Finally, the errors can be estimated by comparison with other calculations; see Table 2 and Table 3. Here, we can see that the error is below 0.04 cm^{-1} for the first 20 Morse levels and does not exceed 0.06 cm^{-1} for the first 60 Aziz levels.

TABLE 3: Vibrational Energy Levels (cm^{-1}) for the Ar_3 with the Aziz Potential

		this work		ref 12		
Γ	v	A_1/E	A_2/E	A_1/E	A_2/E	ref 15 A_1
A_1	0	–254.89		–254.89		–254.89
E	1	–232.36	–232.36	–232.38	–232.38	
A_1	2	–224.28		–224.29		–224.28
A_1	3	–211.94		–211.95		–211.94
E	4	–211.82	–211.81	–211.83	–211.83	
A_1	6	–198.23				–198.24
A_1	8	–193.50				–193.51
A_1	11	–186.26				–186.30
A_1	13	–182.24				–182.26
A_1	15	–177.11				–177.13
A_1	17	–173.50		–173.52		–173.51
E	18	–173.42	–173.42	–173.43	–173.43	
A_1	19	–172.71		–172.75		–172.73
E	20	–172.39	–172.37	–172.42	–172.42	
E	21	–171.78	–171.78	–171.79	–171.79	
A_1	22	–171.60		–171.61		–171.60
A_2	23		–171.15		–171.21	
E	61	–145.81	–145.80	–145.85	–145.85	
A_2	62		–145.76		–145.82	
A_1	63	–145.31		–145.37		
E	64	–144.56	–144.55	–144.64	–144.64	
A_1	65	–144.07		–144.12		

We have also calculated the average rms distances, $\langle r^2 \rangle_v^{1/2}$, that characterize the space extension of the argon trimer. These values were also useful to choose the proper size of the grid required for accurate computations.

Morse Potential. The results for the 20 deepest energy levels for Morse potential are presented in Table 2. Only totally symmetric A_1 states have previously been studied in the literature. The first 10 symmetric A_1 states calculated in refs 9−11 are also given in Table 2. For all energy levels, our results are in a good agreement with all previous calculations.[9,10,11] The discrepancies found in ref 8 are corrected in ref 9 with the extension of the expansion basis.

The difference between our results and results of ref 11 does not exceed 0.03 cm^{-1} for the levels below −170 cm^{-1}. Taking into account the accuracy 0.02 cm^{-1} reported in ref 11, the results perfectly agree. For the levels above −170 cm^{-1}, the difference is much bigger. The authors of ref 11 remarked that their approach based on distributed Gaussian basis was problematic near the barrier to linearity that can be estimated about −170 cm^{-1}. This threshold is clearly visible in Figure 1 that illustrates the distribution of the Ar_3 states.

The comparison of our results with refs 9 and 10 reveals good agreement for all energy levels. The results agree within the 0.05 cm^{-1} error bar.

Aziz Potential. In Table 3, our results for the potential of Aziz are compared with the energy levels calculated in ref 12 and ref 15. In ref 12 by Wright and Hutson, they applied the DVR method in the Jacobi coordinate system, which allowed them to obtain reliable results near the isomerization threshold. The reported accuracy is 0.05 cm^{-1}. Table 3, presenting a selection of the first 66 states, shows that the difference between the same energy levels does not exceed 0.06 cm^{-1} for the first

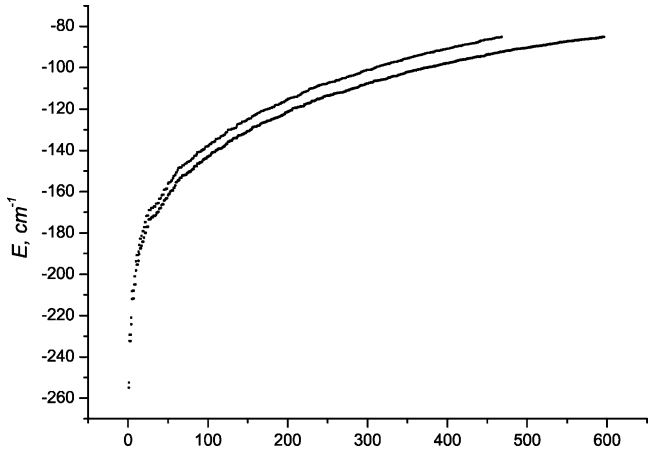

Figure 1. Eigenvalue distribution of the argon trimer. The top line corresponds to the Morse potential; the bottom line, to the Aziz potential. The isomerization barrier to linearity is visible around −170 cm^{-1}.

TABLE 4: Average rms Radii (Å) for the Ar_3 Vibrational Levels

	v	Morse	Aziz
A_1	0	3.91	3.91
E	1	3.98	3.99
A_1	2	3.99	4.00
A_1	3	4.02	4.03
E	4	4.05	4.06
E	5	4.05	4.06
A_1	6	4.10	4.12
E	7	4.18	4.20
A_1	8	4.10	4.11
A_2	9	4.19	4.09
E	10	4.16	4.18
A_1	11	4.18	4.21
E	12	4.29	4.30
A_1	13	4.22	4.23
E	14	4.25	4.27
A_1	15	4.52	4.50
E	16	4.60	4.58
A_1	17	5.59	4.67
E	18	4.85	5.00
A_1	19	4.80	4.52

60 levels. The selection coincides with that of ref 12 for the sake of comparison.

The authors of ref 15 used row-orthonormal hyperspherical coordinates and an expansion of the wave function in terms of hyperspherical harmonics for calculation of the A_1 states. Comparing our energies with these results, we can see that agreement for the first 10 states is even better. For most of the levels, the difference does not exceed 0.02 cm^{-1} while reaches 0.04 cm^{-1} for one level only. This comparison proves good agreement between all results. With the accuracy achieved we are able to distinguish energy levels away from the dissociation threshold.

In Figure 1, the energy level distribution is shown. We can see a great increase in the level density near the isomerization barrier to linearity. While there are only about 20 states below this barrier, the density close to the energy $E \simeq -110$ cm^{-1} is about 6 states/cm^{-1}. Such a high density makes upper states harder to distinguish.

In Table 4 and Figure 2, the rms radii for a few lower energy levels are presented. It can be seen that they increase regularly with the energy below the isomerization barrier. Near the barrier and above it, the behavior becomes highly irregular. Due to these irregularities, the rms radii can be rather different for

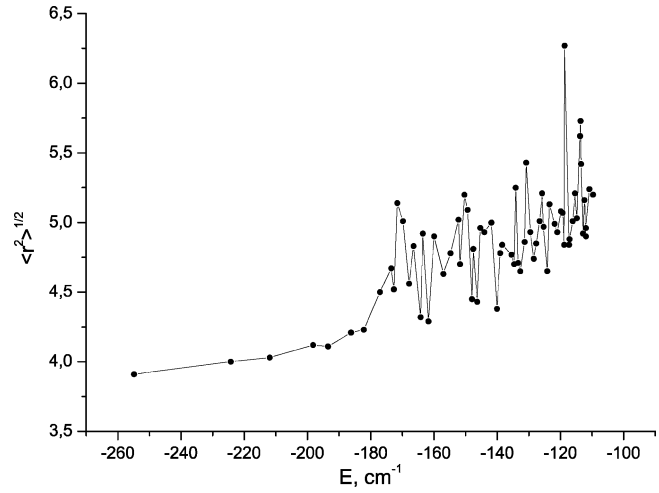

Figure 2. Average rms radii (Å) for the Ar_3 symmetric A_1 states with the Aziz potential.

different potentials while they nearly coincide below the barrier as shown in Table 4. One can also see in Figure 2 that there exist few very extended states the radii of which are considerably larger than radii of neighboring states.

Results for Nonzero Total Angular Momentum. For calculations with the nonzero total momentum, we used the same grid that was used for the zero momentum calculation. Namely, each component s of the total wave function $\psi^{(Js)}$ has been expanded according to eq 4 with the parameters mentioned in the previous section. The only difference is the using of the associated Legendre polynomials $P_i^s(\phi)$ of the order s for the angular variable. The parity is the good quantum number, so we are to solve two independent sets of linear equations. They consist of $(J + 1)$ and J components for the positive and negative parity, respectively. As the same basis is used independently for each component, we do not expect big changes in the accuracy of the calculations.

For the zero momentum calculations, we were able to split all the states into symmetric and antisymmetric sets with respect to the permutation of atoms 2 and 3. As the off-diagonal block operators in eq 1 is antisymmetric with respect to the angle, we can make the similar splitting for the nonzero momentum also. Therefore, if we use the even Legendre polynomials for the $s = 0$ component, we only need odd polynomials for the $s = 1$ component, even polynomials for the $s = 2$ component etc. The analogous intermittent parity behavior we find for the odd polynomials in the zeroth component.

The described splitting has two important advantages. First, it reduces two times the matrix size to compute. Secondly, it greatly facilitates the level classification, giving symmetric and antisymmetric ones in the separate calculation runs.

In Table 5, we present our results for the first four rovibrational levels up to $J = 2$. They include all the levels for both nondegenerated (E_0, E_2, E_3) and degenerated E_1 states. We also note that the accuracy for the calculations can be estimated using the degeneracy properties of the system. In our case, the levels corresponding to the rotationless A_1 states are doubly degenerated for nonzero values of K. We can see in Table 5 that this is true for E_0 and E_2 states while E_3 state experiences a considerable splitting, i.e., a calculation error up to 0.03 cm^{-1}.

Unfortunately, we cannot make the direct comparison with available data because the rotational calculations with the Aziz potential without three-body forces are not accessible. However, we can try to estimate the rotational part of the energies. If we

TABLE 5: Rovibrational Energy Levels (cm^{-1}) for the Ar_3 with the Aziz Potential

J	K	$E_0(A_1)$	$E_1(A_1)$	$E_1(A_2)$	$E_2(A_1)$	$E_3(A_1)$
0	0	–254.89	–232.36	–232.36	–224.28	–211.94
1	0	–254.77	–232.25	–232.25	–224.17	–211.83
	1	–254.81	–232.30	–232.30	–224.21	–211.81
	1	–254.81	–232.25	–232.24	–224.20	–211.80
2	0	–254.54	–232.03	–232.03	–223.94	–211.60
	1	–254.57	–232.07	–232.07	–223.98	–211.59
	1	–254.57	–232.03	–232.01	–223.98	–211.56
	2	–254.68	–232.18	–232.18	–224.09	–211.70
	2	–254.68	–232.02	–232.02	–224.09	–211.69

assume that the three-body forces act on different s-components in a similar way, we can refine rotational excitations of the same vibrational state from the three-body corrections. Then we can compare these excitations with those presented in Table III of ref 15. Our results for the differences $E(J = 2, K = 0) - E(J = 0, K = 0)$ are equal to 0.35, 0.34, and 0.34 cm^{-1} for E_0, E_2, and E_3, respectively. The corresponding results of ref 15 are given by 0.35, 0.34, and 0.34 cm^{-1}, which shows excellent agreement for these rotational excitations.

Assignment of specific quantum numbers to the rovibrational spectrum may pose a complicated problem. In our calculations, the only good quantum numbers are the vibrational state number υ, the total angular momentum J and the parity. The total angular momentum projection K can also be used to label the bound states while it is not a conserved quantum number. In this approach, we do not have other expansion parameters that are physically meaningful. This means that we should analyze the spatial structure of the wave function to assign some additional approximate quantum numbers to the energy level. We do not address this question here.

The rotational structure of the nondegenerated energy levels for the symmetric planar trimer is given by[29]

$$F_{[\nu]}(J,K) = B_{[\nu]}(J(J+1) - K^2/2) \tag{5}$$

The rotational constant $B_{[\nu]}$ in an average during the vibration and thus depends on the vibrational level. If we assign the K number with eq 5, we can see that the rovibrational levels E_0, E_2, and E_3 are perfectly described by this equation. The fitting error is less than 0.01 cm^{-1}.

For higher vibrational levels, the validity of eq 5 becomes questionable,[15] and this equation cannot be used for the level classification. A more accurate way of the level classification was discussed in ref 7. In this way, we consider the norm distribution of the wave function components $\psi^{(Js)}$ with respect to s and attribute the center of this distribution to K. This attribution is meaningful for a narrow distribution only, otherwise K can hardly be assign to the level with a flat norm distribution.

Statistical Analysis

The density of the argon trimer levels above the linearity barrier is rather high. Their wave function structure is quite complicated, and the quantum number assignment is problematic.[12] All this makes it feasible and meaningful to study the statistical properties of the trimer energy levels.

It is known that the classical dynamics of a rotationless Ar_3 cluster is defined by its energy. Three different energy ranges are known for the cluster with pairwise Lennard-Jones potentials.[18] At the lowest energies, the dynamics is nearly regular, but this energy range, below lowest vibrational level, is not accessible in the quantum mechanical system. The next energy range reaches the isomerization barrier. Very few levels of the quantum trimer in this range prevent us from performing a statistical analysis here. Only the energy range above the barrier to linearity is accessible for the statistical analysis of the quantum system.

Prior to the statistical analysis, it is essential to "unfold" the spectrum, i.e., make the average density of the energy levels uniform over the entire energy range.[30,31] To calculate a new set of energy levels $\{\tilde{E}_0, \tilde{E}_1, ..., \tilde{E}_n\}$ from the old set $\{E_0, E_1, ..., E_n\}$, two different unfolding procedures have been used. The reason is that the unfolding procedure, $\tilde{E} = \Phi(E)$, is ambiguous as it includes a functional parameter. Then the meaningful statistical results should be stable with respect to the unfolding. Choosing two different unfolding procedures, we have a possibility to compare the results and check their reliability. We have also verified the translation invariance of our results, i.e., their stability with respect to small changes in the energy range.

The first unfolding procedure requires fitting the integrated level density

$$N(E) = \sum_{i=0}^{n} \Theta(E - E_i) \tag{6}$$

where $\Theta(E)$ is the Heaviside step function, by a polynomial function

$$F(E) = \sum_{l=0}^{3} a_l E^l \tag{7}$$

Unfolded energy levels are then given by

$$\tilde{E}_i = F(E_i) \tag{8}$$

Another approach gives the unfolded spectrum by dividing all the level spacings by the local average spacing

$$\tilde{E}_{i+1} = \tilde{E}_i + (2k+1)\frac{E_{i+1} - E_i}{E_{j_2+1} - E_{j_1}} \tag{9}$$

Here $j_1 = \max(0, i-k)$, $j_2 = \min(n-1, i+k)$. In this work we have used $k = 3$ as in ref 18.

The unfolded spectrum $\tilde{E}_i$ of constant level density can be used for various statistical tests. To estimate short-range correlations between the energy levels, the nearest neighbor level spacings distribution (NNSD)[32] has been used. The NNSD $P(s)$ is the distribution of the nearest neighbor level spacings between

two consecutive levels normalized with respect to the average level spacing. The spectral rigidity $\Delta_3(r)$[30] has been used to diagnose long-range correlations between the levels in an interval of energy E, $E + r$. The spectral rigidity is the mean square deviation from the straight line of the unfolded set $\{(i, \tilde{E}_i)\}$, and is given by equation

$$\Delta_3(r) = \min_{A,B} \frac{1}{r} \int_E^{E+r} (N(\tilde{E}) - A\tilde{E} - B)^2 \, d\tilde{E} \qquad (10)$$

Here r gives also the mean number of energy levels as the mean level spacing is normalized to 1. As the spectral rigidity depends on a few levels contained in the energy interval $(E, E + r)$ only, we have averaged this value throughout the unfolded spectrum of interest.[18]

For the classical system with the regular dynamics, the level statistics in the semiclassical limit is proven to be the Poissonian.[32] Then the NNSD and Δ_3 statistics have the form

$$P(s) = \exp(-s) \qquad (11)$$

$$\Delta_3(r) = \frac{r}{15} \qquad (12)$$

For the chaotic classical Hamiltonian, $\Delta_3(r)$ is identical to that of the Gaussian orthogonal ensemble (GOE):[32]

$$\Delta_3(r) = \frac{1}{\pi^2}(\log(r) - 0.0687) \qquad (13)$$

with a standard deviation of ± 0.11. The NNSD follows the Wigner distribution

$$P(s) = \frac{\pi s}{2} \exp\left(-\frac{\pi s^2}{4}\right) \qquad (14)$$

For systems that are intermediate, i.e., neither completely chaotic nor completely regular, Brody proposed[33] the following distribution for the NNSD

$$P(s,\omega) = As^{\omega} \exp(-\alpha s^{1+\omega}) \qquad (15)$$

where

$$A = (1 + \omega)\alpha \qquad \alpha = \Gamma^{1+\omega}\left(\frac{2 + \omega}{1 + \omega}\right)$$

We have performed the statistical analysis for the E, A_1, and A_2 levels. Results for the A_2 levels resemble those for other symmetries, so we do not show them for the sake of compactness.

In Figures 3 and 4, the Δ_3 values are plotted. For small values of r, all distributions are close to the value obtained from (12), which is the random sequence of levels. On the other hand, the Δ_3 statistic is a typical measure for long-range order in a spectrum; hence it becomes important only for larger values of r. Starting from values $r = +4$ to -5, the Aziz spectrum follows the law (13) for the Gaussian orthogonal ensemble. The energy levels for both E and A_1 representations give similar results. Still one can notice that the A_1 levels closely follow the Wigner distribution while the distribution for the E levels is intermediate between the Poisson and Wigner ones while essentially closer to the latter. The pictures for the Morse potential are qualitatively similar. However, statistic for both representations are clearly intermediate with A_1 levels being little bit closer to the Wigner distribution.

To plot the NNSD (Figures 5 and 6), we have used 59 and 89 energy levels for A_1 and E representations, respectively. The NNSD were fitted by the Brody distribution with the parameter ω representing the measure of the system stochasticity. The histograms show that for the Aziz potential, the level distributions perfectly fit the GOE distribution for both E and A_1 levels. The corresponding ω parameters are fitted to be 0,92 and 1,0, respectively. For the Morse potential, the ω parameters are calculated to be 0.37 and 0.55 for E and A_1 levels, respectively. These values confirm the observation about the intermediate type of the level distribution for the Morse potential. This means that the dynamics of this system is a mixture of regular and chaotic motions.

We have also calculated the correlation coefficient for adjacent first-order spacings[31]

$$C(1) = (\sum_i [S_i(1) - D_1][S_{i+1}(1) - D_1]) \times (\sum_i [S_i(1) - D_1]^2)^{-1} \qquad (16)$$

Here $S_i(1)$ is the first nearest-neighbor spacing, $S_i(1) = E_{i+1} - E_i$, and D_1 is their mean value. This coefficient is known to be $C(1) = -0.271$ for the GOE, and $C(1) = 0$ for the Poisson statistic. In Table 6 we can see that for the Aziz potential,

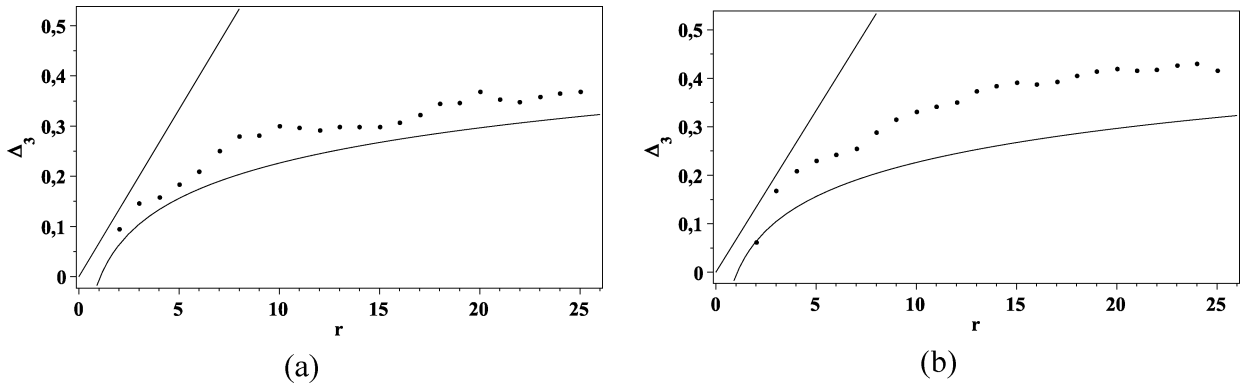

Figure 3. Δ_3 statistic for the E representation for different potentials superimposed with the Poisson (eq 12) and the GOE (eq 13) distributions. (a) Level statistics for the potential of Aziz in the range -173.4 to -109.6 cm^{-1}. A total of 89 energy levels are included. (b) Level statistics for the Morse potential in the energy range from -172 to -110 cm^{-1}. A total of 73 energy levels are included.

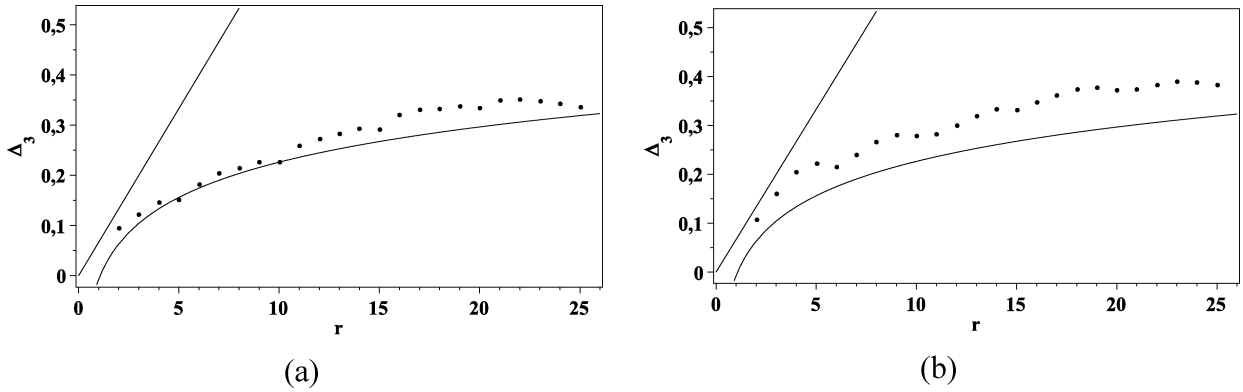

Figure 4. Δ_3 statistic for the A_1 representation for different potentials superimposed with the Poisson (eq 12) and the GOE (eq 13) distributions. A total of 59 energy levels in the interval $[-173.5, -109]$ cm^{-1} are included for the Aziz potential (a). A total of 49 energy levels in the interval $[-172, -111]$ cm^{-1} are included for the Morse potential (b).

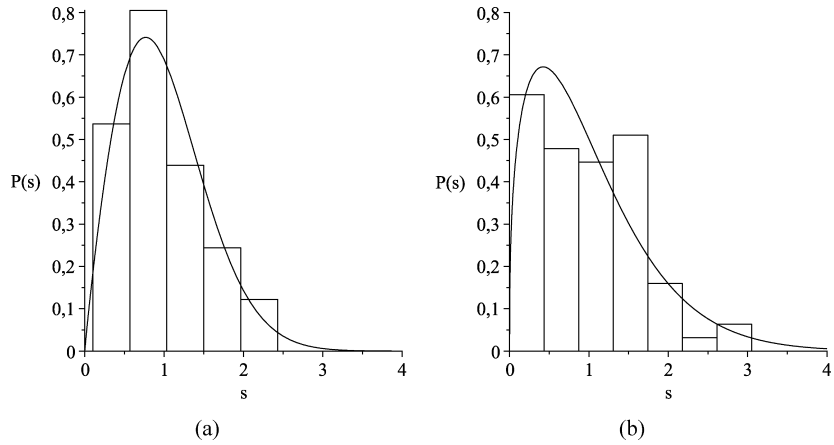

Figure 5. Nearest neighbor level spacing distributions for the E representation superimposed by the Brody distribution (eq 15). (a) NNSD for the Aziz potential with 89 levels included. (b) NNSD for the Morse potential with 73 levels included. The parameter ω was fitted to be 0.92 and 0.37, respectively.

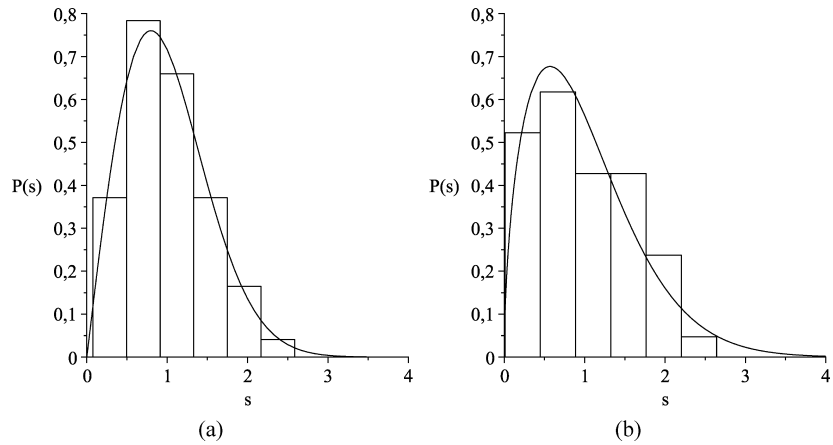

Figure 6. Nearest neighbor level spacing distributions for the A_1 representation for (a) the Aziz potential with 59 levels included and (b) the Morse potential with 49 levels included. The parameter ω was fitted to be 1.0 and 0.55, respectively.

statistics are intermediate to Poisson and GOE. We note that when we decrease the energy range for $C(1)$ calculations, the correlation coefficient also decreases and stabilizes at the value $C(1) = -0.26$ for the E levels. Hence the distribution perfectly resembles the GOE distribution.

For the Morse potential, $C(1)$ are below the GOE value. Recalling then for a level sequence with two alternating constant spacings, $C(1) = -1$,[31] we can expect signs of a regular structure in this case. However, one should remember that the precision of numerical results of $C(1)$ is worse than for Δ_3 and the NNSD, so the additional careful study may be necessary to rely upon these data.

TABLE 6: Correlation Coefficients for Adjacent First-Order Spacings $C(1)$

	E	A_1
Aziz potential	–0.19	–0.14
Morse potential	–0.29	–0.38

Comparing our results for the Aziz and Morse potentials with those for the Lennard-Jones potentials,[18] we can see some

dependence of the level statistics on the pairwise interactions. While the level distributions for the Aziz and Lennard-Jones potentials are rather close to the Wigner distribution, that for the Morse potential is clearly intermediate to Poisson and Wigner; i.e., dynamics is a mixture of regular and chaotic motion. One reason for this difference could be different behavior of the potentials at large distances, affecting high vibrational states.

Conclusions

In this paper we have studied the rovibrational spectrum of the argon trimer for two different potentials. Firstly we can see that our numerical approach, the three-dimensional finite element method, is able to accurately calculate the spectrum of triatomic molecules with many levels of interest, at least up to a few hundred. This makes it feasible to use this approach for studying various systems, both rotationless systems and systems with nonzero total momentum.

Comparing two potentials for the trimer, we can see two distinct ranges in the spectrum. For the deepest levels, both potentials are fitted to give similar (while distinct) eigenvalues. For higher excited vibrational states, however, this similarity breaks. The number of levels and the order of levels with respect to the symmetry representation are completely different, especially above the isomerization barrier. This difference is also reflected in the statistical characteristics of the spectrum while in both cases, the level distributions are intermediate between the Poisson and Wigner ones. For the Aziz potential (as well as for the Lennard-Jones potential[18]) the level distribution is rather close to the Wigner one, and the system exhibits stochastic behavior similar to the Gaussian orthogonal ensemble. For the Morse potential, dynamics found to be a mixture of regular and chaotic motion.

Acknowledgment. This work is supported by Swedish Research Council. E.Y. acknowledges support from the Swedish Institute, Stockholm University, and from the Intel Inc. with the grant "Computation of bound states and resonances of quantum few-body systems on multi-core architectures".

References and Notes

(1) Schinke, R. *Photodissociation Dynamics*; Cambridge University Press: Cambridge, U.K., 1995.
(2) Demtröder, W. *Molecular Physics, Theoretical principles and Experimental Methods*; John Wiley and Sons: New York, 2006.
(3) Tang, J.; Xu, Y.; McKellar, A. R. W.; Jäger, W. *Science* **2002**, *297*, 2030.
(4) Horn, T. R.; Gerber, R. B.; Valentini, J. J.; Ratner, M. A. *J. Chem. Phys.* **1991**, *94*, 6728.
(5) Cooper, A. R.; Jain, S.; Hutson, J. M. *J. Chem. Phys.* **1993**, *98*, 2160.
(6) Hutson, J. M.; Jain, S. J. *J. Chem. Phys.* **1989**, *91*, 4197.
(7) Elander, N.; Levin, S. B.; Yarevsky, E. *Int. J. Quantum Chem.* **2009**, *109*, 459.
(8) González-Lezana, T.; Rubayo-Soneira, J.; Miret-Artés, S.; Gianturco, F. A.; Delgado-Barrio, G.; Villareal, P. *J. Chem. Phys.* **1999**, *110*, 9000.
(9) Baccarelli, I.; Gianturco, F. A.; González-Lezana, T.; Delgado-Barrio, G.; Miret-Artés, S.; Villarreal, P. *J. Chem. Phys.* **2005**, *122*, 144319.
(10) Roy, P. N. *J. Chem. Phys.* **2003**, *119*, 5437.
(11) Garashchuk, S.; Light, J. C. *J. Chem. Phys.* **2001**, *114*, 3929.
(12) Wright, N. J.; Hutson, J. M. *J. Chem. Phys.* **1999**, *110*, 902.
(13) Axilrod, B. M.; Teller, E. *J. Chem. Phys.* **1943**, *11*, 299.
(14) Axilrod, B. M. *J. Chem. Phys.* **1951**, *19*, 724.
(15) Karlický, F.; Lepetit, B.; Kalus, R.; Gadéa, F. X. *J. Chem. Phys.* **2007**, *126*, 174305.
(16) Márquez-Mijares, M.; González-Lezana, T.; Roncero, O.; Miret-Artés, S.; Delgado-Barrio, G.; Villarreal, P. *Chem. Phys. Lett.* **2008**, *460*, 417.
(17) Márquez-Mijares, M.; Pérez, R.; González-Lezana, T.; Roncero, O.; Miret-Artés, S.; Delgado-Barrio, G.; Villarreal, P.; Baccarelli, I.; Gianturco, F. A.; Rubayo-Soneira, J. *J. Chem. Phys.* **2009**, *130*, 154301.
(18) Leitner, D. M.; Berry, R. S.; Whitnell, R. M. *J. Chem. Phys.* **1989**, *91*, 3470.
(19) Curtiss, C. F.; Hirschfelder, J. O.; Adler, F. T. *J. Chem. Phys.* **1950**, *18*, 1638.
(20) Salci, M.; Levin, S. B.; Elander, N.; Yarevsky, E. *J. Chem. Phys.* **2008**, *129*, 134304.
(21) Novaro, O. *Found. Chem.* **2008**, *10*, 3.
(22) Aziz, R. A. *J. Chem. Phys.* **1993**, *99*, 4518.
(23) Herman, P. R.; LaRoque, P. E.; Stoicheff, B. P. *J. Chem. Phys.* **1988**, *89*, 4535.
(24) Elander, N.; Yarevsky, E. *Phys. Rev. A* **1997**, *56*, 1855.
(25) Scrinzi, A. *Comput. Phys. Commun.* **1995**, *86*, 67.
(26) Saad, Y. *Numerical Methods for Large Eigenvalue Problems*; Halsted Press: New York, 1992.
(27) Schenk, O.; Gärtner, K. *J. Future Generation Comput. Syst.* **2004**, *20*, 475.
(28) Elander, N.; Levin, S.; Yarevsky, E. *Phys. Rev. A* **2003**, *67*, 062508.
(29) Herzberg, G. *Molecular Spectra and Molecular Structure II, Infrared and Raman Spectra of Polyatomic Molecules*; Krieger Publishing Co.: Malabar, FL, 1991; pp 22−37, 400−446.
(30) Dyson, F. J.; Mehta, M. L. *J. Math. Phys.* **1963**, *4*, 701.
(31) Haller, E.; Köppel, H.; Cederbaum, L. S. *Chem. Phys. Lett.* **1983**, *101*, 3.
(32) Berry, M. V.; Tabor, M. *Proc. R. Soc. London Ser. A* **1979**, *356*, 375.
(33) Brody, T. A.; Flares, J.; French, J. B.; Mello, P. A.; Pandey, A.; Wong, S. S. *Rev. Mod. Phys.* **1981**, *53*, 385.

JP905109C